

Evidence for Nonpolar Alignment of $[\text{NbOF}_5]^{2-}$ Anions in $\text{Cd}(\text{pyridine})_4\text{NbOF}_5$ Chains

Paulette C. R. Guillory, Janet E. Kirsch,[†] Heather K. Izumi, Charlotte L. Stern, and Kenneth R. Poeppelmeier*

Department of Chemistry, 2145 Sheridan Road, Northwestern University, Evanston, Illinois 60208-3113

Received July 13, 2005; Revised Manuscript Received September 10, 2005

ABSTRACT: A new phase of $\text{Cd}(\text{py})_4\text{NbOF}_5$ ($\text{py} = \text{pyridine}$) (**A**) is a rare example of a mixed metal oxide fluoride in an ordered linear chain structure. This phase is of particular interest because it is a polymorph of a previously reported $\text{Cd}(\text{py})_4\text{NbOF}_5$ phase (**B**) that crystallizes in disordered linear chains. The ordered polymorph **A** contains two distinct Cd^{2+} sites: one which is coordinated to the oxide ligands from two $[\text{NbOF}_5]^{2-}$ units, and another that is coordinated to two *trans* fluoride ligands. As a result, the structure of polymorph **A** features nonpolar linear chains with locally ordered $[\text{NbOF}_5]^{2-}$ anions. This ordering is explained in terms of the inherent electronic differences between oxide and fluoride ligands. The stabilization provided by π -stacking interactions between pyridine ligands on neighboring chains, as well as the effects of reactant stoichiometry on the general structure of the products in the $\text{CdO} \cdot 1/2\text{Nb}_2\text{O}_5/(\text{HF})_x \cdot \text{py}/\text{H}_2\text{O}$ system, is also discussed. Crystal data for the ordered $\text{Cd}(\text{py})_4\text{NbOF}_5$ polymorph: monoclinic space group $P2_1/c$ (No. 14) with $a = 14.097(1)$ Å, $b = 16.353(1)$ Å, $c = 10.4380(9)$ Å, $\beta = 95.569(2)^\circ$, and $Z = 4$.

Introduction

Out-of-center distortions are observed in Group 5 and 6 metal oxide fluoride octahedra with the general formula of $[\text{MO}_x\text{F}_{6-x}]^{n-}$ ($x = 1$, $\text{M} = \text{V}^{5+}$, Nb^{5+} , Ta^{5+} , $n = 2$; $x = 2$, $\text{M} = \text{Mo}^{6+}$, W^{6+} , $n = 2$; $x = 3$, $\text{M} = \text{Mo}^{6+}$, $n = 3$). In each molecular anion, the d^0 metal cation is displaced toward either the corner (C_4 , $x = 1$), edge (C_2 , $x = 2$), or face (C_3 , $x = 3$) of the octahedron occupied by oxide ligands. This displacement is referred to as a “primary” distortion, as it is not directly dependent upon the extended bonding network of the molecular anion in the solid state. Primary distortions in metal oxide fluorides arise from the inherent differences between $\text{M}=\text{O}$ and $\text{M}-\text{F}$ bonding that allow for strong $d\pi-p\pi$ metal–oxide orbital interactions.¹ When $[\text{MO}_x\text{F}_{6-x}]^{n-}$ anions bond with $[\text{M}'\text{L}_4]^{2+}$ ($\text{M}' = \text{Cu}^{2+}$, Zn^{2+} , Cd^{2+} ; $\text{L} = \text{pyridine}$, 3-aminopyridine) cations, solid-state bond network interactions between the anion and the extended structure induce additional changes or “secondary” distortions. Short $\text{M}=\text{O}$ bonds, long $\text{M}-\text{F}$ bonds *trans* to the oxides, and bond angles that deviate from 90° are characteristic of octahedra that have undergone primary and/or secondary distortions. Owing to their inherent asymmetry, these Group 5 and 6 metal oxide fluorides appear to be ideal “building blocks” for the synthesis of noncentrosymmetric (NCS) materials.

The synthesis and characterization of a new linear chain-forming $\text{Cd}(\text{py})_4\text{NbOF}_5$ ($\text{py} = \text{pyridine}$) phase (**A**), as illustrated in Figure 1a, are reported and discussed below. This phase is a polymorph of a previously reported $\text{Cd}(\text{py})_4\text{NbOF}_5$ structure (**B**) (Figure 1b) which exhibits disorder on the oxide and *trans* fluoride sites within the $[\text{NbOF}_5]^{2-}$ units.² Owing to the crystallographic similarities between oxide and fluoride, their identification is often in question, yet the structure–property relationships that exist in these materials make an unambiguous assignment of the oxide and five fluoride ligand sites in coordinated $[\text{NbOF}_5]^{2-}$ anions particularly important. Primary and secondary distortions, as well as the desirable physical and chemical properties associated with these distortions, are only

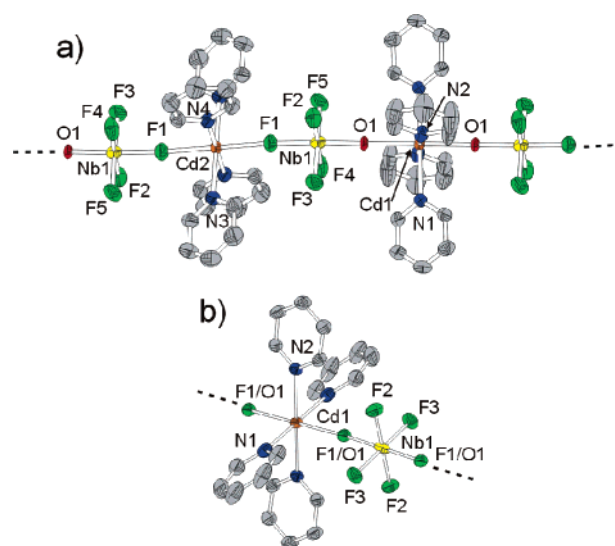


Figure 1. (a) A fragment of the ordered $\text{Cd}(\text{py})_4\text{NbOF}_5$ linear chain polymorph **A** which illustrates the two unique Cd^{2+} coordination environments. (b) A fragment of polymorph **B** with disorder on the oxide and *trans* fluoride ligand sites.

observable in structures without disorder.³ The oxide/fluoride site ambiguity within $\text{Cd}(\text{py})_4\text{NbOF}_5$ has been alleviated by the combined analyses of multiple experimental and theoretical techniques.

Differences in the electronegativities and oxidation states of oxide and fluoride ligands create an inherent dipole moment within individual $[\text{MO}_x\text{F}_{6-x}]^{n-}$ anions. In $[\text{NbOF}_5]^{2-}$ this dipole is collinear to the $\text{O}=\text{Nb}-\text{F}$ bond axis. When polar $[\text{NbOF}_5]^{2-}$ units coordinate to $[\text{M}'\text{L}_4]^{2+}$ cations through the oxide and *trans* fluoride to form a linear chain structure, three long-range structural schemes are possible: a nonpolar chain, a polar chain, or a statistically disordered chain, all shown in Figure 2. In the nonpolar example (Figure 2a), which is similar to that of the ordered polymorph **A**, $[\text{NbOF}_5]^{2-}$ units are aligned in two different (and opposite) orientations, resulting in complete intrachain cancellation of the dipole moments. In contrast, chains of $\text{Cd}(\text{3-apy})_4\text{NbOF}_5$ (3-apy = 3-aminopyridine) contain

* To whom correspondence should be addressed. E-mail: krp@northwestern.edu.

[†] Department of Chemistry, 1725 State Street, University of Wisconsin-La Crosse, La Crosse, WI 54601-3742.

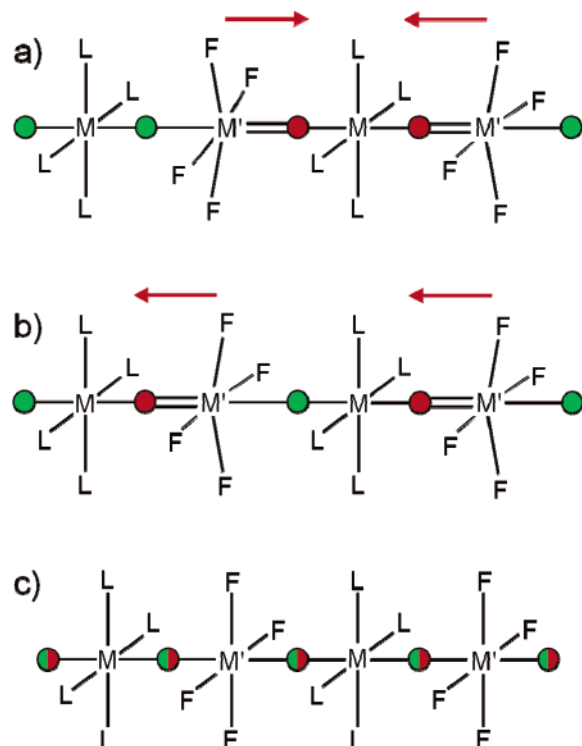


Figure 2. Schematic of the three different ordering schemes possible for a linear chain-forming oxide fluoride compound: (a) nonpolar (individual $[\text{NbOF}_5]^{2-}$ dipoles cancel each other); (b) polar (individual $[\text{NbOF}_5]^{2-}$ dipoles are additive); (c) statistically disordered (individual $[\text{NbOF}_5]^{2-}$ dipoles cannot be observed).

$[\text{NbOF}_5]^{2-}$ anions that are aligned in identical orientations throughout the length of a single chain (Figure 2b).⁴ As a result, the individual dipoles from each $[\text{NbOF}_5]^{2-}$ unit combine additively to form a chain with a net dipole moment. Finally, a nonpolar chain also results when the oxide and *trans* fluoride sites are disordered (Figure 2c) since the dipoles from individual $[\text{NbOF}_5]^{2-}$ units, although still present, cannot be observed in a disordered structure.

The following discussion provides insight into the effects of the extended bond network on the out-of-center distortions displayed by the Nb^{5+} cations and identifies factors that contribute to the specific alignment of $[\text{NbOF}_5]^{2-}$ units in the ordered polymorph **A**. The contributions of the pyridine ligands to the long range (interchain) ordering of individual linear chains via π -stacking interactions are also examined.

Experimental Section

Caution. $(\text{HF})_x$ -pyridine is toxic, corrosive, and must be handled with extreme caution and the appropriate protective gear! If contact with the liquid or vapor occurs, proper treatment procedures should be followed immediately.^{5–7}

Materials. CdO (99%, Aldrich), Nb_2O_5 (99.99%, Aldrich), pyridine (99.8%, anhydrous, Aldrich), and $(\text{HF})_x$ -pyridine (pyridinium polyhydrogen fluoride), 70 wt % HF, Aldrich) were used as received.

Synthesis. The ordered $\text{Cd}(\text{py})_4\text{NbOF}_5$ polymorph **A** was synthesized using 9.74×10^{-2} g (7.58×10^{-4} mol) of CdO , 1.01×10^{-1} g (3.79×10^{-4} mol) of Nb_2O_5 , 6.40×10^{-2} g (2.44×10^{-4} mol) of $(\text{HF})_x$ -pyridine, 2.30×10^{-2} g (1.28×10^{-3} mol) of deionized H_2O , and 2.02 g (2.55×10^{-2} mol) of pyridine. All reactants were sealed in Teflon (fluoro(ethylene-propylene) pouches and placed with up to six other pouches into a 125 mL Parr stainless steel pressure vessel that was filled approximately 33% with deionized H_2O as backfill. The pouches were subsequently heated to 150 °C for 24 h and then cooled to room temperature over an additional 24 h. The pouches were removed from the vessel and opened in air. Colorless columnar crystals of **A** were

Table 1. Crystallographic Data for Two Polymorphs of $\text{Cd}(\text{py})_4\text{NbOF}_5$

	ordered (A)	disordered (B) ^a
formula	$\text{C}_{20}\text{H}_{20}\text{CdF}_5\text{N}_4\text{NbO}$	$\text{C}_{20}\text{H}_{20}\text{CdF}_5\text{N}_4\text{NbO}$
<i>a</i> (Å)	14.0965(12)	12.993(1)
<i>b</i> (Å)	16.3530(14)	10.733(1)
<i>c</i> (Å)	10.4380(9)	16.878(3)
β (°)	95.569(2)	97.11(1)
<i>V</i> (Å ³)	2394.8(4)	2335.6(4)
<i>Z</i>	4	4
calculated density (g/cm ³)	1.755	1.799
cell setting	monoclinic	monoclinic
space group	$P 2_1/c$ (No. 14)	$C 2/c$ (No. 15)
crystal description	columnar	plate
crystal color	colorless	colorless
formula weight	632.71	632.71
<i>R</i> (F) ^b	0.040	0.026
<i>R</i> _w (F) ^c	0.092	0.031
software used	SHELXTL	TEXSAN

^a Ref 2. ^b $R = \sum |F_o| - |F_c| / \sum |F_o|$. ^c $R_w = [\sum w(F_o^2 - F_c^2) / \sum w(F_o^2)]^{1/2}$.

collected by filtration and were characterized by either single crystal or powder XRD and FTIR.

Crystallographic Determination. Single-crystal X-ray data were collected with Mo $K\alpha$ radiation ($\lambda = 0.71073$ Å) on a Bruker SMART-1000 CCD diffractometer and integrated with the SAINT-Plus program.⁸ The structures were solved by direct methods and expanded using Fourier techniques in the SHELXTL program.⁹ A face-indexed absorption correction was applied using the XPREP program. Structures were checked for missing symmetry elements with the PLATON program.¹⁰ All non-hydrogen atom sites were located from the difference map and refined anisotropically. Hydrogen atoms, located exclusively on the pyridine rings, were placed in calculated positions ($\text{C}-\text{H} = 0.95$ Å and $\text{N}-\text{H} = 0.88$ Å) and were refined using a riding model. Isotropic displacement parameters were constrained to equal 1.2 times the equivalent isotropic displacement parameter of the parent atoms. Crystallographic data and selected bond distances for $\text{Cd}(\text{py})_4\text{NbOF}_5$ polymorph **A** and the disordered polymorph **B** are given in Tables 1 and 2.

Powder X-ray Diffraction. Powder XRD data were recorded with a Rigaku RINT 2000 diffractometer (Cu $K\alpha$ radiation) operating at 40 keV and 20 mA. The diffraction patterns were recorded over the angular range $5^\circ \leq 2\theta \leq 50^\circ$ in 0.05° increments with 1 s counting.

Infrared Spectroscopy. Samples were ground with KBr and pressed into a pellet. Mid-IR (400–4000 cm^{-1}) spectra were collected using a Bio-Rad FTS-60 FTIR spectrometer operating at a resolution of 2 cm^{-1} .

Computational Study. Electronic structure calculations based on the crystallographically determined coordinates for the ordered $\text{Cd}(\text{py})_4\text{NbOF}_5$ linear chain and the $[\text{pyH}]_2[\text{Cd}(\text{py})_4(\text{NbOF}_5)_2]$ cluster¹¹ structures were carried out using the Fenske–Hall molecular orbital method.¹² Owing to the inherent approximations made by this self-consistent, approximate Hartree–Fock type method, geometry optimization is not possible; however, the results of FH calculations provide a reliable and detailed description of the bonding environment of any atom in the molecular fragment within a reasonable amount of computational time. A truncated chain unit consisting of three $[\text{NbOF}_5]^{2-}$ anions alternating with two $[\text{Cd}(\text{py})_4]^{2+}$ cations served as a model for $\text{Cd}(\text{py})_4\text{NbOF}_5$, while the $[\text{pyH}]_2[\text{Cd}(\text{py})_4(\text{NbOF}_5)_2]$ cluster was modeled by a single $[(\text{NbOF}_5)(\text{Cd}(\text{py})_4)(\text{NbOF}_5)]^{2-}$ unit. See Supporting Information for input atomic coordinates.

All atomic basis functions were obtained by a best fit to Herman–Skillman atomic calculations¹³ using the method of Bursten, Jensen, and Fenske.¹⁴ The 5s and 5p functions were given exponents of 2.2 for Nb and Cd. Valence p functions for C, N, O, and F were retained as double- ζ functions, while all other functions were reduced to single- ζ functions. Hydrogen was assigned an exponent of 1.2.

Bond valence calculations were carried out for the $[\text{pyH}]_2[\text{Cd}(\text{py})_4(\text{NbOF}_5)_2]$ cluster and the ordered $\text{Cd}(\text{py})_4\text{NbOF}_5$ polymorph.¹⁵ Atomic charges and overlap populations were calculated via Mulliken population analyses.^{16,17} In this methodology, electronic charges are assigned according to the atomic orbital coefficients of normalized molecular wave functions that are represented as LCAOs (linear combination of atomic orbitals). Despite the simplicity of Mulliken and bond valence

Table 2. Selected Bond Lengths and Bond Valence Sums^a for the Ordered and Disordered^b Polymorphs of Cd(py)₄NbOF₅ and for the Anionic Cluster [pyH]₂[Cd(py)₄(NbOF₅)₂]^c

bond	length (R _i , Å)	valence S _i ^d	residual charge	bond	length (R _i , Å)
ordered Cd(py) ₄ NbOF ₅ (A)			disordered Cd(py) ₄ NbOF ₅ (B)		
Nb=O1	1.8841(19)	1.08	0.92*	Nb–O1/F1	1.925(1)
Nb–F1	1.9619(19)	0.68	0.32*	Nb–F2 × 2	1.902(1)
Nb–F2	1.909(2)	0.79	0.21	Nb–F3 × 2	1.930(1)
Nb–F3	1.911(2)	0.79	0.21		
Nb–F4	1.913(2)	0.78	0.22		
Nb–F5	1.901(2)	0.81	0.19	Cd–O1/F1	2.291(1)
	ΣS _{Nb}	4.93		Cd–N1 × 2	2.354(2)
				Cd–N2 × 2	2.333(2)
Cd1–O1	2.2731(19)				
Cd1–N1 × 2	2.315(3)				
Cd1–N2 × 2	2.369(3)				
Cd2–F1	2.2753(19)				
Cd2–N3 × 2	2.365(3)				
Cd2–N4 × 2	2.362(3)				
[pyH] ₂ [Cd(py) ₄ (NbOF ₅) ₂]					
Nb=O1	1.750(6)	1.54	0.46*		
Nb–F1 × 2	1.932(3)	0.74	0.26		
Nb–F2 × 2	1.936(3)	0.74	0.26		
Nb–F3	2.095(4)	0.48	0.52**		
	ΣS _{Nb}	4.98			

^a Bond valences calculated with the program Bond Valence Calculator v. 2.00, C.Hormillosa, S. Healy and T. Stephen, McMaster University (1993). ^b Ref 2. ^c Ref 11. ^d Valence sums calculated with the formula $S_i = \exp[(R_0 - R_i)/B]$ where S_i = bond valence of bond i , R_0 = constant dependent upon the bonded elements, R_i = bond length of bond i , and $B = 0.370$. ΣS_{Nb} = bond valence sum for the metal. Residual charge on ligand $i = V_i - S_i$, where V_i = oxidation state of ligand i . (*) denotes a ligand bonded to Cd²⁺; (**) denotes a ligand coordinated by [pyH]⁺ cations.

analyses, both methods provide a sufficient level of accuracy in describing general trends exhibited by the closely related structures compared below.

Results

Unit Cell Comparison of the Cd(py)₄NbOF₅ Polymorphs.

Exact bond length determinations within a crystal are possible when all atomic positions reflect crystallographic order. Although oxide and fluoride are too similar in atomic number to be distinguishable via X-ray techniques, the asymmetric coordination environment of the [NbOF₅]²⁻ anions in polymorph **A** is commensurate with an ordered linear chain structure composed of alternating [NbOF₅]²⁻ and [Cd(py)₄]²⁺ ions. The Nb=O bond length of 1.8841(19) Å falls between the short Nb=O bond at 1.750(6) Å in the [pyH]₂[Cd(py)₄(NbOF₅)₂] cluster compound¹¹ and the longer 1.914(3) Å Nb=O bond reported in linear chains of Cd(3-apy)₄NbOF₅ (3-apy = 3-aminopyridine).⁴ Similarly, the *trans* Nb–F bond length of 1.9619(19) Å is both shorter than that in the cluster (Table 2) and longer than the 1.937(3) Å bond in Cd(3-apy)₄NbOF₅. The [NbOF₅]²⁻ octahedra in polymorph **A** are aligned such that the oxide and *trans* fluoride ligands on each unit coordinate to a different [Cd(py)₄]²⁺ cation. The specific ligand ordering of the [NbOF₅]²⁻ anions along each infinite chain results in two unique cadmium sites with O–Cd1–O and F–Cd2–F local bonding environments, as illustrated in Figure 1a. When these chains pack together in the solid state, they are aligned to one another such that the Cd1 centers within a single chain are surrounded by Cd2 centers from nearest neighbor chains (Figure 3). The asymmetry of the Nb=O and *trans* Nb–F bond lengths eliminates inversion centers on the niobium sites.

The fundamental structural unit of the disordered polymorph **B** is also an infinite linear chain composed of alternating anionic [NbOF₅]²⁻ octahedra and cationic [Cd(py)₄]²⁺ metal–ligand complexes, as shown in Figure 1b; however, the [NbOF₅]²⁻ octahedra in polymorph **B** are disordered on the *trans* ligand sites, O and F1. As a result of this disorder, the reported metal–ligand bond lengths listed in Table 2 are averaged and a center of symmetry is retained on the niobium sites.

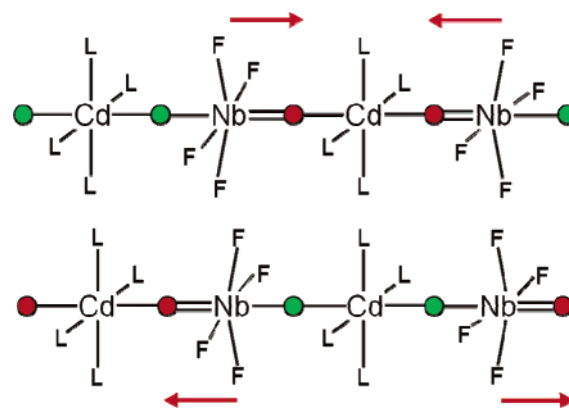


Figure 3. The specific alignment of the Cd1 and Cd2 sites in neighboring chains of the ordered polymorph **A**.

Despite similarities in the local structures of the two polymorphs, they differ significantly in their long-range order and crystal packing. Polyhedral representations of the linear chains, as shown in Figure 4, illustrate the different crystal structures of the two polymorphs. All of the chains in ordered polymorph **A** are parallel to one another and display a hexagonal packing pattern. In contrast, parallel chains of disordered polymorph **B** pack in sheets. These sheets are rotated by an angle of 90° every $c/2$. The different long-range order exhibited by the two polymorphs results in distinct unit cells and densities. Ordered polymorph **A** crystallizes in the monoclinic space group $P2_1/c$ with a unit cell volume of 2395(4) Å³ and a calculated density of 1.76 g/cm³, while disordered polymorph **B** crystallizes in the monoclinic space group $C2/c$ with a smaller unit cell volume of 2336(4) Å³ and a slightly higher calculated density of 1.80 g/cm³.

The infrared spectra for both polymorphs show a characteristic band for [NbOF₅]²⁻. In polymorph **A** this band occurs at $\nu_s(\text{Nb=O}) = 922 \text{ cm}^{-1}$ and thus is slightly shifted from the previously reported value of $\nu_s(\text{Nb=O}) = 901 \text{ cm}^{-1}$ in the disordered polymorph.²

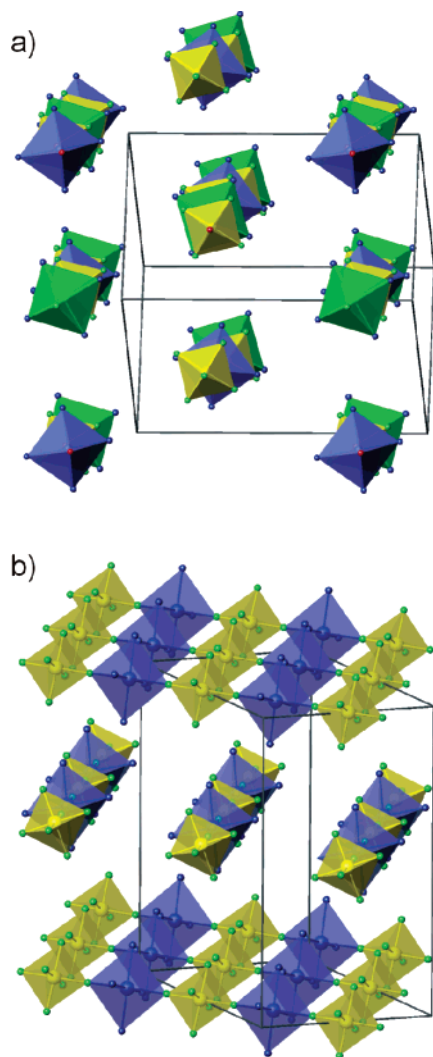


Figure 4. Three-dimensional packing of the (a) ordered and (b) disordered polymorphs of $\text{Cd}(\text{py})_4\text{NbOF}_5$. Yellow octahedra represent $[\text{NbOF}_5]^{2-}$ units, while green and blue octahedra represent crystallographically distinct $[\text{Cd}(\text{py})_4]^{2+}$ units. Pyridine rings have been omitted for clarity.

Table 3. Calculated Mulliken Charges^a

	$[\text{pyH}]_2[\text{Cd}(\text{py})_4(\text{NbOF}_5)_2]$ cluster	$\text{Cd}(\text{py})_4\text{NbOF}_5$ chain	$\text{Cd}(\text{3-apy})_4\text{NbOF}_5$ chain ^b
O	-0.916	-0.914	-0.920
<i>trans</i> F	-0.637	-0.570	-0.557
<i>equat.</i> F ^c	-0.545	-0.535	-0.537
Nb	+1.874	+1.813	+1.808
Cd	+0.980	+0.976	+0.883

^a SCF convergence limit = 0.001. ^b Ref 4. ^c Average value for all four equatorial F⁻.

Calculations. Residual charges as determined by bond valence calculations and Mulliken atomic charges for different compounds are given in Tables 2 and 3, respectively.

Discussion

Although disorder in the ligand sites of $[\text{MO}_x\text{F}_{6-x}]^{n-}$ anions is a common occurrence in mixed metal oxide fluorides, $[\text{NbOF}_5]^{2-}$ octahedra have been successfully ordered previously. For example, $[\text{NbOF}_5]^{2-}$ anions within the discrete “cluster” compound, $[\text{pyH}]_2[\text{Cd}(\text{py})_4(\text{NbOF}_5)_2]$,¹¹ are completely ordered. An ordered linear chain structure has also been reported for the

aforementioned $\text{Cd}(\text{3-apy})_4\text{NbOF}_5$.⁴ The sites occupied by oxide or fluoride ligands in an $[\text{NbOF}_5]^{2-}$ anion can often be identified by a comparison of the six metal–ligand bond lengths around the Nb^{5+} center; $\text{Nb}=\text{O}$ bonds are typically around 1.8 Å in length, while $\text{Nb}-\text{F}$ interactions, particularly those *trans* to $\text{Nb}=\text{O}$ bonds, tend to be 1.9 Å or longer.

Previous work with mixed-metal oxide fluorides that incorporate noncentrosymmetric $[\text{MO}_x\text{F}_{6-x}]^{n-}$ anions has demonstrated that these units preferentially coordinate to cationic species through the oxide or fluoride ligand(s) with the most negative charge.^{2,18–20} Individual atomic charges can be evaluated in ordered crystal structures using methods such as bond valence theory or Mulliken population analyses. These methods confirm that a $[\text{NbOF}_5]^{2-}$ anion coordinates to a cationic species both through its oxide ligand and through the fluoride *trans* to the $\text{M}=\text{O}$ bond, as these are typically the two ligands with the most negative charges.

Polymorphism. Although the ordered and disordered $\text{Cd}(\text{py})_4\text{NbOF}_5$ polymorphs exhibit markedly different crystal packing, both structures are constructed from chemically similar units. Thus, the relationship between the structures of ordered and disordered $\text{Cd}(\text{py})_4\text{NbOF}_5$ chains is not only polymorphic, but somewhat polytypic, as well. Polytypes, which can be thought of as “one-dimensional polymorphs”,^{21,22} are crystalline solids that consist of identical major structural units, such as chains or sheets, that are linked together in different ways.^{23,24} As there are typically many different ways to link layers or chains together, numerous polytypes may exist for a single polymorph.^{25–29}

The existence of polymorphism and polytypism in mixed metal oxide fluoride materials provides an additional and interesting variable to be considered in targeted and rational syntheses of materials with specific chemical and physical properties.^{30,31} In particular, one polymorph of a material may exhibit NLO behavior that is not seen in the other polymorph that forms. Although polymorphs are typically prepared through different synthetic routes, the term *concomitant* polymorphism describes the formation of polymorphs within the same chemical preparation under identical reaction conditions.^{32,33} The existence of concomitant polymorphs, as well as the complex combination of thermodynamic and kinetic factors that favor the formation of one structure over another, can provide insight into the stability of a particular structure type. The $\text{Cd}(\text{py})_4\text{NbOF}_5$ polymorphs that are the focus of this paper are concomitant, as they form in the same preparation.

This work is focused primarily on the ordered $\text{Cd}(\text{py})_4\text{NbOF}_5$ polymorph, but it is important to note that the local ligand order in disordered polymorph **B** has been investigated further using solid-state NMR techniques.³⁴ Grey and co-workers found a single resonance in the ¹¹³Cd MAS NMR spectrum of disordered $\text{Cd}(\text{py})_4\text{NbOF}_5$, indicative of locally ordered linear chains that contain $[\text{NbOF}_5]^{2-}$ anions aligned in a polar manner (similar to the chain shown in Figure 2b). The ¹⁹F MAS NMR spectrum, however, exhibited two resonances, and therefore supports either a polar or nonpolar local structural model for the disordered polymorph. On the basis of these results, the disordered polymorph most likely consists of linear chains that are ordered locally (*intra*chain order) but pack together in a disordered manner (*inter*chain disorder). This is in marked contrast to polymorph **A**, which exhibits both intra- and interchain ordering.

Bond Network Effects on the $[\text{NbOF}_5]^{2-}$ Primary Distortion. As noted earlier, discrete, molecular fragments of the oxide fluoride compounds served as models for these computational studies. This approximation is similar to the finite-cluster

approximation that is frequently made in computational studies of adsorbate-covered surfaces.^{35,36} The model for the $\text{Cd}(\text{py})_4\text{NbOF}_5$ linear chain compound consisted of five octahedra (three anions alternated with two cations). At this size, the effects of chain termination are less significant than on smaller models, yet the chain is still short enough to keep the number of basis functions tractable.

We recently reported the structural and electronic effects of the extended bond network on the primary distortions exhibited by $[\text{NbOF}_5]^{2-}$ anions in linear chains of $\text{Cd}(3\text{-apy})_4\text{NbOF}_5$.⁴ The results of electronic structure calculations indicated, as expected, that as the oxide fluoride anionic species participated in more extensive solid-state interactions, the magnitude of the primary distortion decreased. This magnitude was determined by comparisons of the calculated charges on the oxide and fluoride ligands, as well as the calculated $\text{Nb}=\text{O}$ and *trans* $\text{Nb}-\text{F}$ bond overlap populations in compounds that represented three different structure types: a hypothetical uncoordinated $[\text{NbOF}_5]^{2-}$ anion,³ the $[\text{pyH}]_2[\text{Cd}(\text{py})_4(\text{NbOF}_5)_2]$ cluster compound,¹¹ and the linear chain-forming $\text{Cd}(3\text{-apy})_4(\text{NbOF}_5)$ compound. A similar analysis of $\text{Cd}(\text{py})_4\text{NbOF}_5$ polymorph **A** indicates that this compound follows the trend of decreased distortion with increasing solid-state contacts to the anion.

The extended bond network surrounding a $[\text{NbOF}_5]^{2-}$ anion has a noticeable effect on the $\text{Nb}=\text{O}$ and *trans* $\text{Nb}-\text{F}$ bond lengths and, in turn, on the amount of electron density localized on the oxide and *trans* fluoride ligands. Each $[\text{NbOF}_5]^{2-}$ unit in the ordered $\text{Cd}(\text{py})_4\text{NbOF}_5$ linear chain participates in covalent bonds to two Cd^{2+} centers through its oxide and *trans* fluoride ligands. This increased coordination simultaneously lengthens the $\text{Nb}=\text{O}$ bonds and shortens the *trans* $\text{Nb}-\text{F}$ bonds in the linear chain polymorph relative to the cluster compound, as indicated by the bond lengths in Table 2. Bond valence calculations and Mulliken charges both indicate that the oxide ligands retain substantial negative charges in the $[\text{pyH}]_2[\text{Cd}(\text{py})_4(\text{NbOF}_5)_2]$ cluster and in $\text{Cd}(\text{py})_4\text{NbOF}_5$ polymorph **A**, but the shortening of the *trans* $\text{Nb}-\text{F}$ bonds is accompanied by an decrease in the negative charge localized on the *trans* fluoride ligands. The bond network surrounding the $[\text{NbOF}_5]^{2-}$ anions appears to have less of an effect on the equatorial $\text{Nb}-\text{F}$ bond lengths and equatorial ligand charges; there is a contraction of only ~ 0.02 Å in the equatorial $\text{Nb}-\text{F}$ bond lengths in the ordered polymorph compared to those in the cluster compound.

Bond overlap populations are a measure of the strength of covalent interactions between two atoms: larger overlap populations correspond to more strongly covalent bonds.¹⁷ A graphical comparison of the $\text{Nb}=\text{O}$ and *trans* $\text{Nb}-\text{F}$ bond overlap populations in the hypothetical uncoordinated $[\text{NbOF}_5]^{2-}$ anion, the $[\text{Cd}(\text{py})_4(\text{NbOF}_5)_2]^{2-}$ cluster fragment, and the ordered $\text{Cd}(\text{py})_4\text{NbOF}_5$ polymorph, as well as the individual σ and π contributions to each bond, is given in Figure 5. In the uncoordinated $[\text{NbOF}_5]^{2-}$ anion, π interactions between Nb 4d and O 2p orbitals constitute more than half of the total $\text{Nb}=\text{O}$ bond strength. Figure 5 shows that this π contribution is slightly lower in the $[\text{pyH}]_2[\text{Cd}(\text{py})_4(\text{NbOF}_5)_2]$ cluster, where the oxide ligands form additional bonds to a Cd^{2+} center and the *trans* fluoride ligands act as hydrogen bond acceptors for the $[\text{pyH}]^+$ cations. In the linear chain compound, both the oxide and *trans* fluoride ligands are bonded to Cd^{2+} and Nb^{5+} centers, and the π contributions to the $\text{Nb}=\text{O}$ bonds are significantly decreased. At the same time, however, the bar plots in Figure 5 show that σ contributions to the $\text{Nb}=\text{O}$ bonds are relatively unaffected by the extent of the $[\text{NbOF}_5]^{2-}$ coordination. These data

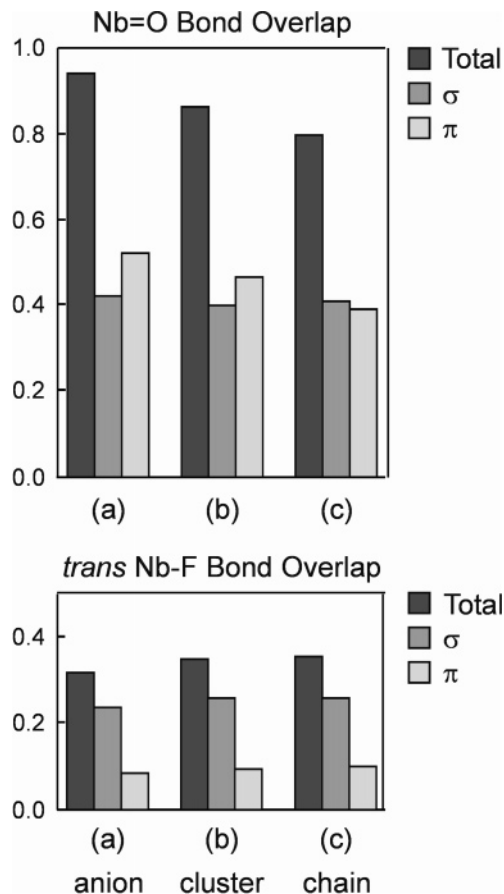


Figure 5. Comparison of the relative $\text{Nb}=\text{O}$ and *trans* $\text{Nb}-\text{F}$ bond strengths (based on calculated bond overlap populations), as well as the individual σ and π contributions to each, in (a) uncoordinated $[\text{NbOF}_5]^{2-}$ (see ref 3), (b) $[\text{pyH}]_2[\text{Cd}(\text{py})_4(\text{NbOF}_5)_2]$, and (c) the ordered $\text{Cd}(\text{py})_4\text{NbOF}_5$ polymorph.

therefore confirm that any decrease in the primary distortion of $[\text{NbOF}_5]^{2-}$ comes from a weakening of the $\text{Nb}=\text{O}$ $d\pi-p\pi$ interaction.

The $\text{CdO}\cdot 1/2\text{Nb}_2\text{O}_5/(\text{HF})_x\cdot \text{py}/\text{H}_2\text{O}$ Composition Space. Crystallized metal oxide fluoride products from multiple hydrothermal reactions can be conveniently and methodically analyzed via a composition space diagram, which is similar to a ternary phase diagram in which the solid products are analyzed.^{19,37} Analysis of a composition space diagram allows for a direct comparison of the effects that different initial reactant amounts have on the composition or phase(s) of the final products. Composition space diagrams for the $\text{CdO}\cdot 1/2\text{Nb}_2\text{O}_5/(\text{HF})_x\cdot \text{py}/\text{H}_2\text{O}$ system were constructed by placing different molar ratios of the reactant metal oxides, $(\text{HF})_x\cdot \text{py}$, and H_2O in Teflon pouches. Solid phase products were subsequently characterized using FTIR spectroscopy and powder XRD. A powder XRD spectrum of each $\text{Cd}(\text{py})_4\text{NbOF}_5$ polymorph with minor phase components has been included in Supporting Information. Composition prisms were then constructed by directly comparing multiple composition space diagrams with varying amounts of solvent (pyridine).³⁷⁻³⁹

Similar to an earlier analysis of this system,² several regions of selective crystal growth can be identified within the $\text{CdO}\cdot 1/2\text{Nb}_2\text{O}_5/(\text{HF})_x\cdot \text{py}/\text{H}_2\text{O}/\text{pyridine}$ composition prism (Figure 6). In the bottom left corner of each composition space, high concentrations of $(\text{HF})_x\cdot \text{py}$ prevent the crystallization of any species, while the large mole fractions of metal oxides and low concentrations of $(\text{HF})_x\cdot \text{py}$ in the upper corner of the prism

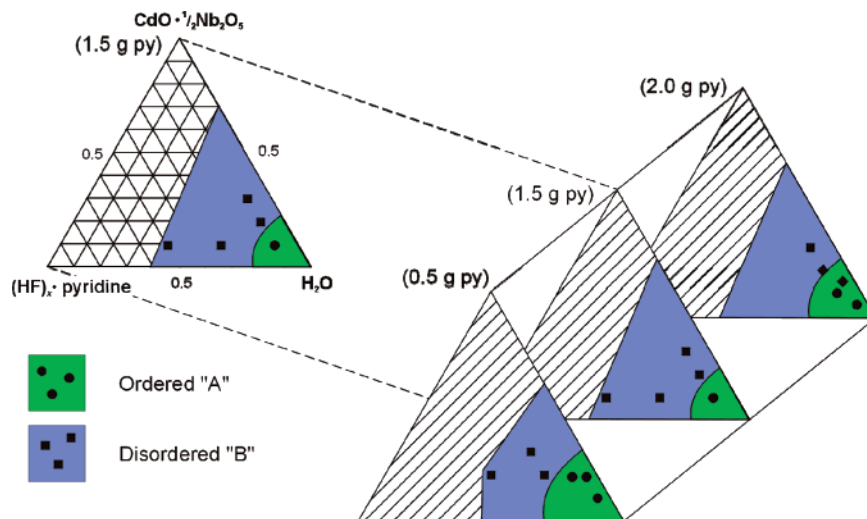


Figure 6. Composition space prism for the $\text{CdO}\cdot\frac{1}{2}\text{Nb}_2\text{O}_5/(\text{HF})_x\cdot\text{py}/\text{H}_2\text{O}$ system. Filled circles (squares) represent reactant molar ratios that resulted in the isolation of the ordered (disordered) $\text{Cd}(\text{py})_4\text{NbOF}_5$ polymorph.

reduce dissolution of the reactants. Crystals of $[\text{pyH}]_2[\text{Cd}(\text{py})_4(\text{NbOF}_5)_2]$ and $\text{Cd}(\text{py})_4\text{NbOF}_5$ form in the remainder of the prism: the formation of the former cluster compound versus the latter linear chain is related to the amount of $(\text{HF})_x\cdot\text{py}$ added to the reaction. At higher HF concentrations the solvent pyridine is protonated, and the presence of $[\text{pyH}]^+$ cations facilitates the crystallization of the cluster species.

Each of the points on the composition prism shown in Figure 6 represent reactant molar ratios in the $\text{CdO}\cdot\frac{1}{2}\text{Nb}_2\text{O}_5/(\text{HF})_x\cdot\text{py}/\text{H}_2\text{O}/\text{pyridine}$ system that have resulted in the crystallization of ordered or disordered $\text{Cd}(\text{py})_4\text{NbOF}_5$ polymorphs. Near the boundaries of each region, either structure is possible. The presence of two polymorphs within a single synthetic route confirms their concomitant polymorphism. Regions where the ordered compound **A** predominantly forms are denoted by the green shaded areas in Figure 6, while the disordered polymorph **B** tends to form in the blue shaded area of the composition prism. The solvent pyridine concentration appears to have little effect on the distribution of solid products in this system; in all three of the composition space diagrams in Figure 6, the ordered polymorph tends to form most readily in the “water-rich” corner. This region is ideal for the formation of linear chain structures because the reduced amount of $(\text{HF})_x\cdot\text{py}$ limits the formation of protonated pyridine.

One of the fundamental questions about any system with two or more concomitant polymorphic structures has to do with the identification of the factors which favor one structure over another. For example, what causes the ordered $\text{Cd}(\text{py})_4\text{NbOF}_5$ polymorph to preferentially form over the disordered structure in the water-rich region of the composition space? Although the composition space prism in Figure 6 indicates little dependence of solid product distribution on the solvent concentration in the 125 mL pressure vessel, such is not the case in the composition prism constructed from a series of reactions carried out in a 2 L pressure vessel (see Supporting Information). Obviously, numerous thermodynamic and kinetic factors affect the distribution of the solid products in the $\text{CdO}\cdot\frac{1}{2}\text{Nb}_2\text{O}_5/(\text{HF})_x\cdot\text{py}/\text{H}_2\text{O}/\text{pyridine}$ system. In the remainder of this discussion, we will focus on two of the main differences between the ordered and disordered $\text{Cd}(\text{py})_4\text{NbOF}_5$ polymorphs: the interchain lattice interactions that result in different crystal packing and the local ordering of the oxide and *trans* fluoride ligands.

Interchain π Stacking Interactions. As discussed above, extended bond network interactions have a significant effect

on the primary distortions of $[\text{MO}_x\text{F}_{6-x}]^{n-}$ anions. Unlike $\text{Cd}(\text{3-apy})_4\text{NbOF}_5$, where neighboring linear chains are held together via an extensive hydrogen bonding network formed by the amino substituents on the 3-aminopyridine ligands, $\text{Cd}(\text{py})_4\text{NbOF}_5$ polymorphs do not have a source of hydrogen bond donors. Instead, the predominant network interactions formed by linear chains of $\text{Cd}(\text{py})_4\text{NbOF}_5$ are interchain π stacking interactions between pyridine rings. Although strong, attractive interactions between π systems are commonly observed experimentally and are well-known conceptually, there have been few models that explain the basic mechanisms of π stacking in terms that can be generalized to different systems. One qualitative approach toward modeling π - π interactions has been put forth by Hunter and Sanders, who developed a series of rules for aromatic-aromatic interactions based on simple charge distributions in π systems.⁴⁰

In general, two main contributions to a π stacking interaction between two aromatic rings have been recognized: attractive forces between the more negative π system on one ring with the more positive σ network on the other, and repulsive forces between the two π systems.⁴⁰ In π systems that contain heteroatoms, such as pyridine, the electron density in the ring is polarized toward the more electronegative atom. This polarization facilitates stronger face-to-face π stacking relative to a phenyl substituent, as the presence of an electron-withdrawing atom decreases the π electron density and in turn the π - π repulsion between the rings.⁴¹ Electrostatically unfavorable π - π interactions are overcome even more effectively when the π orbital cloud of one aromatic ring interacts with the σ hydrogen orbitals on another ring in an edge-to-face, or “T” shaped configuration.⁴² These π - σ interactions are the strongest for rings that are stacked in a completely orthogonal configuration, but also occur between aromatic rings that are tilted less than 90° from each other. Crystals that contain these edge-to-face aromatic interactions are said to pack in “herringbone” structures.⁴²⁻⁴⁴

In the ordered polymorph **A** shown in Figure 7a, the pyridine rings exhibit a herringbone packing. A pyridine ring coordinated to one of the two distinct Cd^{2+} sites interacts with the π system from a pyridine coordinated to the other Cd^{2+} site. Aromatic stacking interactions between nitrogen-containing ligands in metal complexes typically have a centroid-to-centroid distance from 3.3 to 3.8 Å, with an angle between the ligand planes that is 27° on average.⁴¹ In polymorph **A**, the centroid-to-centroid

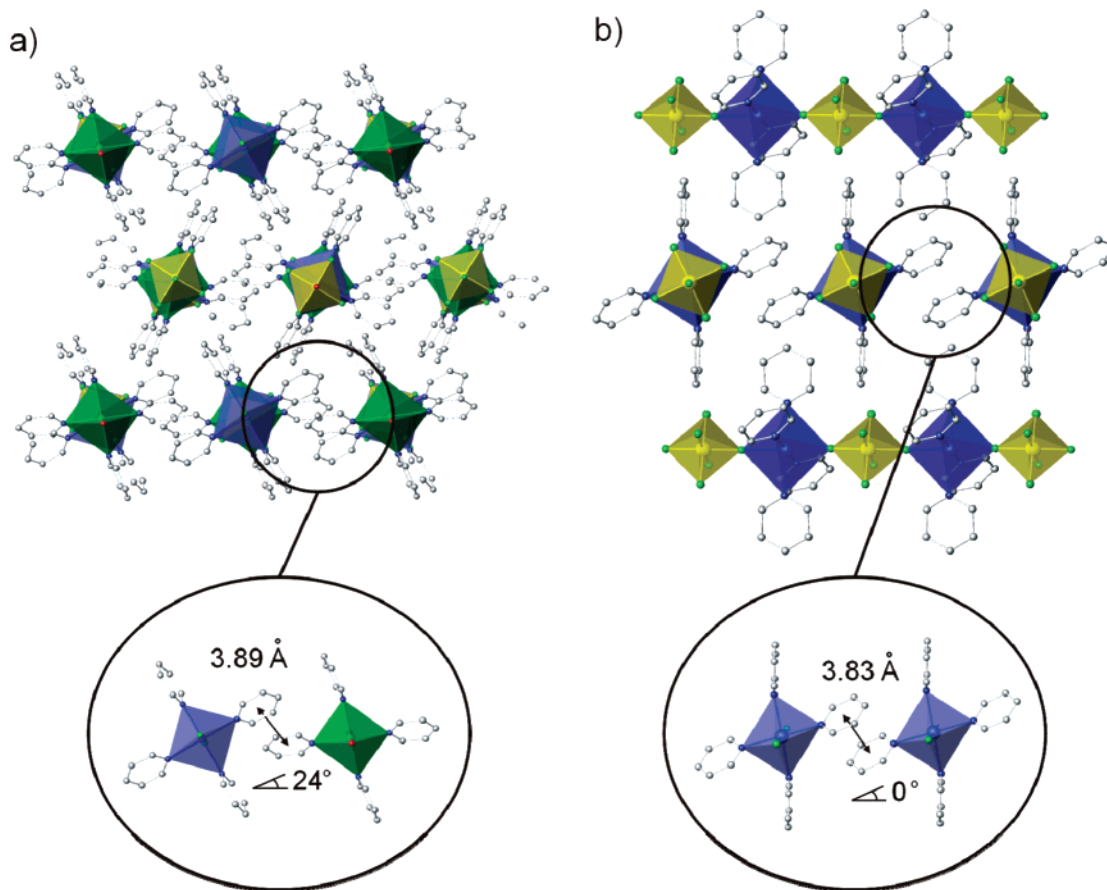


Figure 7. Different π -stacking interactions between pyridine rings on neighboring linear chains of (a) ordered and (b) disordered $\text{Cd}(\text{py})_4\text{NbOF}_5$ polymorphs. Note that the centroid-to-centroid distances are within experimental error by an order of magnitude (Table 1).

distance between the pyridine rings is 3.89 Å and the coplanar angle is 24° . The relative positions of two π -stacking rings indicates that the extended bond network in the ordered polymorph contains elements of both a parallel face-to-face interaction and a π - σ edge-to-face interaction.

In contrast, polymorph **B** is shown in Figure 7b, where the close-up view shows that the pyridine rings on neighboring chains which are spatially related to one another by a center of inversion participate in complete face-to-face coplanar π stacking ($\angle 0^\circ$). The distance between the pyridine rings in the disordered polymorph is slightly shorter, at 3.83 Å and thus is also within a reasonable distance for π - π interactions. The disordered structure is stabilized through these coplanar stacking interactions.⁴¹ Aromatic interactions also contribute to the rotation of the linear chain planes in the packing of the disordered polymorph **B**, as this rotation optimizes the face-to-face π stacking between neighboring chains. The slightly shorter centroid-to-centroid distance, combined with the higher calculated density of the unit cell (see Table 1) suggests, if only qualitatively, that the disordered polymorph packs more efficiently than its ordered counterpart. Such efficiency may contribute to the observation that the disordered polymorph preferentially forms in a larger region of the $\text{CdO} \cdot 1/2\text{Nb}_2\text{O}_5 / (\text{HF})_x \cdot \text{py} / \text{H}_2\text{O} / \text{pyridine}$ composition space.

Local Intrachain Order. It is important to note that the local nonpolar ordering of the $[\text{NbOF}_5]^{2-}$ units in $\text{Cd}(\text{py})_4\text{NbOF}_5$ differs from the polar ordering that has been observed in chains of $\text{Cd}(3\text{-apy})_4\text{NbOF}_5$. This difference may be related to the hard/soft mismatch between the Cd^{2+} centers and the oxide or fluoride ligands. Although both oxide and fluoride are classified as hard bases, fluoride is harder than oxide.⁴⁵ As such, oxide

ligands are more likely to coordinate to the softer Cd^{2+} cation, as they do in the $[\text{pyH}]_2[\text{Cd}(\text{py})_4(\text{NbOF}_5)_2]$ cluster compound. When the Cd^{2+} is coordinated by 3-aminopyridine ligands, however, the electron donating properties of the $-\text{NH}_2$ group lower the actual positive charge on the cadmium, as indicated by the calculated Mulliken charges in Table 3. This softens the cadmium further, which in turn increases its hard/soft mismatch with oxide and fluoride. Thus, $\text{Cd}(3\text{-apy})_4\text{NbOF}_5$ may adopt a polar O-Cd-F intrachain ordering to avoid the formation of highly mismatched F-Cd-F interactions that are inherent to the nonpolar chain structure (see Figure 2a).

When all of the factors presented above are taken into consideration, a hypothetical, stepwise reaction pathway for nonpolar $\text{Cd}(\text{py})_4\text{NbOF}_5$ chain formation can be envisioned. The initial step in the chain formation would involve the coordination of a majority of the $[\text{NbOF}_5]^{2-}$ anions in solution to $[\text{Cd}(\text{py})_4]^{2+}$ cations through their oxide ligands to form $[\text{Cd}(\text{py})_4(\text{NbOF}_5)_2]^{2-}$ cluster-like units. In the absence of solvated pyridinium cations, these units would then coordinate to excess $[\text{Cd}(\text{py})_4]^{2+}$ through their available *trans* fluoride ligands to form an extended linear chain. This mechanism would result in the specific nonpolar ordering that is observed in $\text{Cd}(\text{py})_4\text{NbOF}_5$ polymorph **A**.

Conclusions

Further exploration of the $\text{CdO} \cdot 1/2\text{Nb}_2\text{O}_5 / (\text{HF})_x \cdot \text{py} / \text{H}_2\text{O} / \text{pyridine}$ composition prism has resulted in the synthesis and isolation of a new ordered linear chain compound. The nonpolar intrachain ordering is similar to the ordering of the $[\text{NbOF}_5]^{2-}$ anionic units in the $[\text{pyH}]_2[\text{Cd}(\text{py})_4(\text{NbOF}_5)_2]$ cluster compound, where both negative species are bonded to a Cd^{2+} site through

their oxide ligands; however, in the extended linear chain structure the *trans* fluorides from each $[\text{NbOF}_5]^{2-}$ are also bonded to a second Cd^{2+} center. These additional bond network contacts simultaneously weaken the $\text{Nb}=\text{O}$ $d\pi-p\pi$ overlap while slightly reinforcing the *trans* $\text{Nb}-\text{F}$ interaction. As a result, the magnitude of the inherent primary distortion within the $[\text{NbOF}_5]^{2-}$ anion is decreased relative to that in compounds where $[\text{NbOF}_5]^{2-}$ participates in few, if any, solid state interactions. The results of these studies indicate that the controlled synthesis of linear chain structures with specific polar or nonpolar intrachain order depends strongly on the input molar ratios of the reactants, the reaction conditions, and the nature of the organic ligands coordinated to the late transition metal centers.

Acknowledgment. The authors gratefully acknowledge support from the National Science Foundation (Solid State Chemistry Award Nos. DMR-9727516 and DMR-0312136), the Illinois Minority Graduate Research Incentive, and the use of the Central Facilities supported by the MRSEC program of the National Science Foundation at the Materials Research Center of Northwestern University (Award No. DMR-0076097).

Supporting Information Available: One X-ray crystallographic information file in CIF format including atomic coordinates, anisotropic thermal parameters, interatomic distances and angles; two powder XRD spectra that show the ordered and disordered polymorphs with their minor solid-phase products; one list of input atomic coordinates for FH calculations in PDF format; one composition space diagram for the $\text{CdO}\cdot\frac{1}{2}\text{Nb}_2\text{O}_5(\text{HF})_x\cdot\text{py}/\text{H}_2\text{O}$ system in a 2 L pressure vessel. This material is available free of charge via the Internet at <http://pubs.acs.org>.

References

- Kunz, M.; Brown, I. D. *J. Solid State Chem.* **1995**, *115*, 395–406.
- Halasyamani, P. S.; Heier, K. R.; Norquist, A. J.; Stern, C. L.; Poeppelmeier, K. R. *Inorg. Chem.* **1998**, *37*, 369–371.
- Welk, M. E.; Norquist, A. J.; Arnold, F. P.; Stern, C. L.; Poeppelmeier, K. R. *Inorg. Chem.* **2002**, *41*, 5119–5125.
- Izumi, H. K.; Kirsch, J. E.; Stern, C. L.; Poeppelmeier, K. R. *Inorg. Chem.* **2005**, *44*, 884–895.
- Bertolini, J. C. *J. Emerg. Med.* **1992**, *10*, 163–168.
- Peters, D.; Miethchen, R. *J. Fluorine Chem.* **1996**, *79*, 161–165.
- Segal, E. B. *Chem. Health Saf.* **2000**, *7*, 18–23.
- SAINT-Plus*, v. 6.02A.; Bruker Analytical X-ray Instruments, Inc.: Madison, WI, 2000.
- Sheldrick, G. M. *SHELXTL*, v. 5.10; Bruker Analytical X-ray Instruments, Inc.: Madison, WI, 1997.
- Spek, A. L. *PLATON*; Utrecht University: Utrecht, The Netherlands, 2001.
- Halasyamani, P.; Willis, M. J.; Heier, K. R.; Stern, C. L.; Poeppelmeier, K. R. *Acta Crystallogr.* **1996**, *C52*, 2491–2493.
- Hall, M. B.; Fenske, R. F. *Inorg. Chem.* **1972**, *11*, 768–775.
- Herman, F.; Skillman, S. *Atomic Structure Calculations*; Prentice Hall: Englewood Cliffs, NJ, 1963.
- Bursten, B. E.; Jensen, J. R.; Fenske, R. F. *J. Chem. Phys.* **1978**, *68*, 3320–3321.
- Altermatt, D.; Brown, I. D. *Acta Crystallogr.* **1985**, *B41*, 240–244.
- Mulliken, R. S. *J. Chem. Phys.* **1955**, *23*, 1833–1840.
- Mulliken, R. S. *J. Chem. Phys.* **1955**, *23*, 1841–1846.
- Heier, K. R.; Norquist, A. J.; Wilson, C. G.; Stern, C. L.; Poeppelmeier, K. R. *Inorg. Chem.* **1998**, *37*, 76–80.
- Halasyamani, P.; Willis, M. J.; Stern, C. L.; Poeppelmeier, K. R. *Inorg. Chem.* **1996**, *35*, 1367–1371.
- Welk, M. E.; Norquist, A. J.; Stern, C. L.; Poeppelmeier, K. R. *Inorg. Chem.* **2000**, *39*, 3946–3947.
- Verma, A. R.; Krishna, P. *Polymorphism and Polytypism in Crystals*; Wiley: New York, 1966.
- Verma, A. R.; Trigunayat, G. C. In *Solid State Chemistry*; Rao, C. N. R., Ed.; Marcel Dekker: New York, 1974; pp 51–94.
- Smith, J. V. *Geometrical and Structural Crystallography*; John Wiley & Sons: New York, 1982; p 328.
- Wells, A. F. *Structural Inorganic Chemistry*, 5th ed.; Oxford University Press: New York, 1984.
- Braga, D.; Abati, A.; Scaccianoce, L.; Johnson, B. F. G.; Grepioni, F. *Solid State Sci.* **2001**, *3*, 783–788.
- Braga, D.; Cojazzi, G.; Paolucci, D.; Grepioni, F. *CrystEngComm* **2001**, *38*, 1–3.
- Gavezzotti, A. *CrystEngComm* **2002**, *4*, 343–347.
- Masciocchi, N.; Ardizzoia, G. A.; La Monica, G.; Moret, M.; Sironi, A. *Inorg. Chem.* **1997**, *36*, 449–454.
- Masciocchi, N.; Bruni, S.; Cariati, E.; Cariati, F.; Galli, S.; Sironi, A. *Inorg. Chem.* **2001**, *40*, 5897–5905.
- Vrcelj, R. M.; Shepherd, E. E. A.; Yoon, C.-S.; Sherwood, J. N.; Kennedy, A. R. *Cryst. Growth Des.* **2002**, *2*, 609–617.
- Herbstein, F. H. *Cryst. Growth Des.* **2004**, *4*, 1419–1429.
- Heier, K. R.; Norquist, A. J.; Halasyamani, P. S.; Duarte, A.; Stern, C. L.; Poeppelmeier, K. R. *Inorg. Chem.* **1999**, *38*, 762–767.
- Bernstein, J.; Davey, R. J.; Henck, J.-O. *Angew. Chem., Int. Ed.* **1999**, *1999*, 3440–3461.
- Du, L.-S.; Schurko, R. W.; Kim, N.; Grey, C. P. *J. Phys. Chem. A* **2002**, *106*, 7876–7886.
- Johnson, B. F. G.; Gallup, M.; Roberts, Y. V. *J. Mol. Catal.* **1994**, *86*, 51–69.
- Koper, M. T. M.; Van Santen, R. A.; Neurock, M. In *Catalysis and Electrocatalysis at Nanoparticle Surfaces*; Wieckowski, A., Savinova, E. R., Vayenas, C. G., Eds.; Marcel Dekker: New York, 2003; pp 1–34.
- Norquist, A. J.; Heier, K. R.; Stern, C. L.; Poeppelmeier, K. R. *Inorg. Chem.* **1998**, *37*, 6495–6501.
- Harrison, W. T. A.; Dussack, L. L.; Jacobson, A. J. *J. Solid State Chem.* **1996**, *125*, 234–242.
- Norquist, A. J.; Welk, M. E.; Stern, C. L.; Poeppelmeier, K. R. *Chem. Mater.* **2000**, *12*, 1905–1909.
- Hunter, C. A.; Sanders, J. K. M. *J. Am. Chem. Soc.* **1990**, *112*, 5525–5534.
- Janiak, C. *J. Chem. Soc., Dalton Trans.* **2000**, 3885–3896.
- Jorgensen, W. L.; Severance, D. L. *J. Am. Chem. Soc.* **1990**, *112*, 4768–4774.
- Curtis, M. D.; Cao, J.; Kampf, J. W. *J. Am. Chem. Soc.* **2004**, *126*, 4318–4328.
- Horowitz, G.; Bachet, B.; Yassar, A.; Lang, P.; Demanze, F.; Fave, J.-L.; Garnier, F. *Chem. Mater.* **1995**, *7*, 1337–1341.
- Pearson, R. G. *Chemical Hardness*; John Wiley & Sons: New York, 1997.

CG050331T